Devitrification process of FeSiBCuBbX nanocrystalline alloys: Mössbauer study of the intergranular phase

2000 J. Phys.: Condens. Matter 12 8089

(http://iopscience.iop.org/0953-8984/12/37/308)

J. Phys.: Condens. Matter **12** (2000) 8089–8100. Printed in the UK PII: S0953-8984(00)10832-X

Devitrification process of FeSiBCuBbX nanocrystalline alloys: Mössbauer study of the intergranular phase

J M Borrego†, C F Conde†, A Conde†, V A Peña-Rodríguez‡ and J M Greneche§

† Departamento de Física de la Materia Condensada. Universidad de Sevilla, PO Box 1065, 41080 Sevilla, Spain

‡ Universidad Nacional Mayor de San Marcos, Facultad de Ciencias Físicas, PO Box 14-0149, Lima 14, Peru

§ Laboratoire de Physique de l'Etat Condensé, UPRESA CNRS 6087, Université du Maine, F-72085 Le Mans Cedex 9, France

Received 10 January 2000, in final form 20 June 2000

Abstract. Mössbauer experiments were performed at room temperature using different experimental configurations on several series of nanocrystalline FeSiBCuNbX alloys (X = Zr, Nb, Mo and V) obtained after annealing treatments of melt-spun ribbons. The refinement of Mössbauer spectra allows the kinetics and the local structural rearrangement mechanisms associated with the nanocrystallization process to be compared. The hyperfine field distributions of the intergranular phase show the emergence of a bimodal behaviour that becomes significantly more pronounced from volumetric crystalline fractions estimated at ∼20–25%, regardless of the nature of the substituting element. The hyperfine field distribution can be described by means of two Gaussian components, consistent with of a two-cluster-like model. Such a behaviour can be attributed to the presence of iron-rich and iron-poor zones within the intergranular phase, resulting from the diffusion process. These mechanisms are found to be independent of the nature of X. In addition, strong in-plane magnetic structures are evidenced for Nb-, Mo-, and V-based systems while the magnetic domains tend to be randomly distributed in Zr-based nanocrystalline alloys.

1. Introduction

Nanocrystalline FeSiBCuNb alloys are attractive materials not only from a fundamental point of view due to their structural and magnetic properties, but also from their enormous industrial potentiality due to their excellent soft magnetic properties. The so-called Finemet alloy with composition $Fe_{73.5}Cu_1Nb_3Si_{13.5}B_9$ exhibits to date the best magnetic performance. The microstructure of nanocrystalline alloys obtained after an appropriate annealing treatment of the amorphous precursor consists of ultrafine grains of a few nanometres embedded within a residual amorphous matrix [1, 2]. In order to increase the glass forming ability and to improve the magnetic characteristics of the classic Finemet alloy some attempts were made by substituting some of the elements. The influence of refractory elements addition (X = V, W, Ta, Mo and Zr) in nanocrystalline FeSiBCuNbX alloys with different Fe and Si/B content has been investigated by different experimental techniques. It was found that the thermal stability of the amorphous alloy rises in the order V < Mo < W < Ta ≈ Nb < Zr [3–6]. With respect to the structure the substitution of Nb changes the stable mean grain size of the nanocrystalline Fe,Si phase in the sequence V > Mo > W > Ta ≈ Nb ≈ Zr, an effect which is correlated with the atomic diameter of the elements that increase in the inverse order [3, 5, 6]. The magnetic

0953-8984/00/378089+12$30.00

properties respond in a similar way when Nb atoms are substituted by Ta, W and Mo, whereas the samples containing V do not show so good soft magnetic properties [5]. Similar results are obtained in FeSiBCu alloys in which Nb atoms are completely substituted by the same refractory elements [7–9].

Towards a better understanding of these different behaviours, an experimental approach based on a local technique was developed. The crystalline fraction and the local magnetic hyperfine properties of both the crystalline and the intergranular phases can be evidenced by means of ^{57}Fe Mössbauer spectrometry. Indeed, this technique remains an excellent tool to investigate iron-based heterogeneous systems due to its atomic scale sensitivity. One expects to estimate thus the values of the hyperfine field (B), the isomer shift (δ) and the quadrupolar shift (2ε) characteristics of the crystalline components, the distribution of the hyperfine field and the mean values of the hyperfine parameters and their correlation, if any, with the intergranular matrix, and their respective proportions. Finally the magnetic anisotropy is reflected through the area ratios of the absorption lines from which the value of θ, defined by the directions of the hyperfine field and of the γ-rays, can be obtained. Nevertheless, it is important to emphasize that the description of the hyperfine structure requires great attention during the fitting procedure, as it is a sensitive and delicate stage [10–19].

We mainly report in the present paper the Mössbauer study performed at room temperature first on some as-quenched amorphous $Fe_{73.5}Si_{13.5}B_9CuNbX_2$ (X = V, Mo, Nb, and Zr) alloys and then on several nanocrystalline alloys obtained after different annealing treatments to scan the volumetric crystalline fraction. Great attention is particularly devoted to the hyperfine structure of the intergranular phase versus the volumetric crystalline fraction, which is discussed on the basis of a two-cluster-like model associated with a bimodal hyperfine field distribution. Such a description was widely proposed in the case of as-quenched amorphous alloys but has not been applied yet to describe the amorphous remainder in nanocrystalline alloy, to our knowledge. It is thus now well established that the intergranular phase of most nanocrystalline alloys (including Finemet and Nanoperm) is not homogeneous.

In the experimental section, we briefly present the fitting procedure (detailed in a previous paper [19]), which was successfully applied to Finemet-type nanocrystalline alloys to obtain an insight into the hyperfine structure of both the nanocrystalline grains and the intergranular phase, whatever the volumetric fraction of the crystalline phase is. The present results are then discussed as a function of the volumetric crystalline fraction and of the substituting element X, which originates strongly different crystalline grain size, ranging from about 10 to 25 nm.

2. Experimental section

Amorphous $Fe_{73.5}Si_{13.5}B_9CuNbX_2$ (X = V, Mo, Nb, and Zr) ribbons were first quenched from master alloys using the melt-spinning technique. To obtain different stages of the structural evolution, the ribbons were annealed under a protective atmosphere for 5 and/or 60 minutes at 738, 753, 773, 798, 823 and 873 K; these temperatures were selected by comparison with those of the two crystallization peaks observed from differential scanning calorimetry data [8]. The microstructure of these nanocrystalline alloys was characterized by means of x-ray diffraction at room temperature and transmission electron microscopy. The mean values of the crystalline grain sizes [8, 20] are reported hereafter in the different tables.

Mössbauer spectra were taken in a transmission geometry using a constant acceleration spectrometer with a ^{57}Co(Rh) source. The Mössbauer spectra were fitted with NORMOS [21] and MOSFIT programs [22]. The isomer shift (IS) values are quoted in relation to that of α-Fe at 300 K.

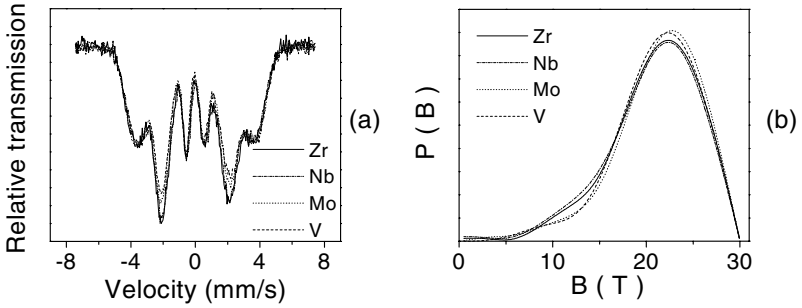

Figure 1. Experimental transmission Mössbauer spectra of the as-quenched samples and their corresponding hyperfine field distributions.

We considered the following fitting procedures which have been recently improved and discussed in [19]. Mössbauer spectra of the as-quenched alloys were fitted by using a discrete distribution of hyperfine parameters, consistent with an amorphous structure (see figure 1). In order to well reproduce the asymmetrical shape of the spectra, it is necessary to introduce a linear correlation between the magnetic hyperfine field and the isomer shift. Indeed, the hyperfine field depends on the magnetic surrounding and the isomer shift on the total s density at the ^{57}Fe nucleus, i.e. the chemical surroundings. Let us note that the linear relationship has no physical meaning. The spectra obtained on the nanocrystalline alloys exhibit a complex hyperfine structure resulting from sharp lines superimposed on broad overlapped lines, which can be attributed to the crystalline phase and the residual amorphous matrix, respectively. The main hyperfine parameters are (i) the values of both the upper and lower limits of the hyperfine field distribution $P(B)$, (ii) the degree of correlation between the hyperfine field and the isomer shift, (iii) the magnetic texture of both the crystalline grains and the residual amorphous matrix assumed to be identical and (iv) the number of sextets to describe the crystalline contribution, i.e the number of iron sites, which is correlated to the Si content. These parameters were optimized from spectra recorded at 300 K under different γ-beam configurations as follows [19]. (i) In-plane saturated magnetic configuration leads to spectra the relative line intensities of which are expected to be 3:4:1:1:4:3. Such a situation can be reached by applying a small magnetic field parallel (higher than the demagnetizing field) to the length of the ribbon and perpendicular to the γ-beam, accounting for the positive magnetostrictive behaviour of present alloys. (ii) 'Free texture spectra' (3:2:1:1:2:3) consistent with a completely random distribution of magnetic moment directions are obtained using the magic-angle configuration (with the γ-beam oriented at $\theta = 55^\circ$ with respect to the ribbon plane) [23]. The values of hyperfine parameters for the crystalline sextets, the hyperfine field distribution of the amorphous remainder and their respective proportions have to be configuration independent. In addition to the use of different configurations, we directly compare the experimental normalized spectra in order to visualize their differences. Such an approach allows us to check qualitatively the increase or decrease of the crystalline fraction and/or the evolution of the hyperfine field distributions of the intergranular phase, if any. By such a way, the estimates of the volumetric crystalline fraction by Mössbauer spectrometry were finally found in a rather good agreement with those deduced from x-ray diffraction.

For thermomagnetic (TMG) experiments the magnetic field of a small magnet ($\sim$15 mT) was applied to the sample and the temperature variation of the magnetic force was recorded as an apparent weight change of the sample. Previous calibration of the thermobalance (Perkin–Elmer TGA-7) was checked by using the Curie points of nickel, perkalloy and iron standards.

Table 1. Curie temperatures and mean values of the hyperfine parameters corresponding to the as-quenched samples and crystallization onset temperatures.

	T_C	$\langle B \rangle$	$\langle \delta \rangle$	$\langle 2\varepsilon \rangle$	$\langle \theta \rangle$	T_{onset}
	(K)	(T)	(mm s^{-1})	(mm s^{-1})	(°)	(K)
X	±5	±5	±0.01	±0.01	±3	±5
Zr	594	20.9	0.10	−0.03	67	797
Nb	592	20.6	0.10	−0.02	67	791
Mo	602	21.3	0.10	−0.01	63	772
V	598	21.1	0.10	0.01	61	763

The values of the Curie temperature of both the amorphous matrix and the crystalline phase were determined by the intersection point of the steepest tangent to the $M(T)$ curve with the T axis or with the magnetization curve extrapolated down to temperatures $T < T_c$, respectively.

3. Mössbauer results and discussion

3.1. As-quenched amorphous alloys

The hyperfine field distributions obtained from Mössbauer spectra of the four alloys in the as-quenched state (see figure 1) reveal the presence of an intense peak around 23 T and a small tail at low hyperfine field values, regardless of the partial substitution. High field values can be ascribed to Fe atoms preferentially surrounded by Fe, Si and B and the low field values to Fe preferentially surrounded by Cu, Nb(X) and B [12]. Table 1 lists the values of the mean hyperfine magnetic field $\langle B \rangle$ and Curie temperature for the four alloys. $\langle B \rangle$ values are, in all cases, significantly lower than those found in the alloys without refractory elements: 23.4 and 23.7 T for FeSiB and FeCuSiB alloys, respectively. Therefore, the addition of refractory elements has the effect of reducing the mean value of the hyperfine magnetic field of the amorphous phase. The resulting mean hyperfine field values at 300 K slightly increase in the same order that the Curie temperatures: Nb < Zr < V < Mo [24].

In addition, the presence of an in-plane texture of magnetic domains can be concluded for the four alloys, but more clearly evidenced in Nb and Zr containing samples. This preferential orientation is consistent with the presence of large quenched-in stresses.

3.2. Low crystalline fraction alloys (<20%)

The early stage of the nanocrystallization process of $Fe_{73.5}Si_{13.5}B_9CuNbX_2$ alloys was studied from as-cast ribbons annealed for 5 and 60 minutes at different temperatures under an argon atmosphere. Figure 2 compares the spectra of the four nanocrystalline samples annealed for 5 minutes at 25 K (Zr, V) and 20 K (Nb, Mo) below their respective crystallization onset temperature (reported in table 1 and in [8]). Their corresponding hyperfine magnetic field distributions are also presented.

Table 2 lists first the increase of the Curie temperature values of the residual amorphous phase relative to the amorphous as-quenched ones and then the hyperfine parameters of both the intergranular and the crystalline phases for Zr and V containing samples. A very small increase in the mean hyperfine field value of the amorphous with respect to that of the initial amorphous can be appreciated, while a significant decrease in the value of θ is observed. These results are related to the changes occurring in the local structure of the Fe neighbourhood during the early stages of the nanocrystallization (with volumetric crystalline fractions $\lesssim$5%).

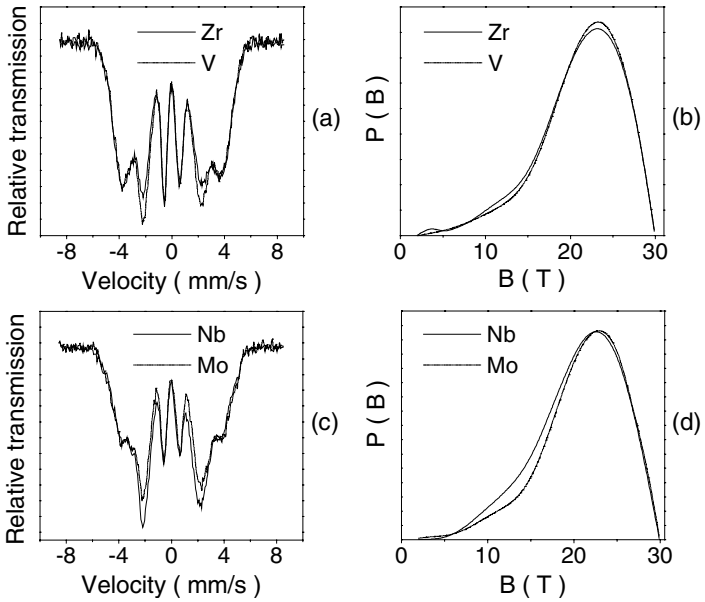

Figure 2. Experimental transmission Mössbauer spectra of the four nanocrystalline samples annealed for 5 minutes at a temperature 25 K (Zr, V) (a) and 20 K (Nb, Mo) (c) below their respective crystallization onset temperature and their corresponding hyperfine magnetic field distributions (b) and (d) respectively.

Table 2. Increment of the values of the Curie temperatures of the residual amorphous phase relative to the initial amorphous and the hyperfine parameters corresponding to both the intergranular and the crystalline phases for samples containing Zr and V annealed at 773 K and 738 K respectively for 5 minutes, and mean size of corresponding crystalline grains.

	Intergranular amorphous phase					Crystalline phase					
	ΔT_C	$\langle B \rangle$	$\langle \delta \rangle$	$\langle 2\varepsilon \rangle$	$\langle \theta \rangle$	B	δ	2ε	θ	CF	$\langle d \rangle$
	(K)	(T)	(mm s^{-1})	(mm s^{-1})	(°)	(T)	(mm s^{-1})	(mm s^{-1})	(°)	(%)	(nm)
X	±5	±3	±0.01	±0.01	±3	±4	±0.04	±0.02	±3	±3	±2
Zr	21	21.3	0.10	−0.02	48	30.9	0.06	−0.03	48	5	11
V	20	21.4	0.10	−0.01	55	30.7	0.07	−0.04	55	5	21

Considering the high diffusivities of some of the present atoms, one expects the emergence of Fe weakly ordered clusters (at this stage the crystalline component is fitted with only one sextet with $H \sim 31$ T) that tends, with addition of diffusive Si atoms, to transform into an FeSi arrangement as embryos of the DO_3 type FeSi crystalline grains [24, 25]. One notes that Fe weakly ordered clusters occur at the early stage of crystallization in Nanoperm alloys, giving rise to a non-zero magnetization above the Curie temperature of the amorphous precursor [26].

In other respects, the change of $\langle \theta \rangle$ and the increase in T_C values of the amorphous phase (∼20 K) are consistent with the relaxation of internal stresses during the first stages of crystallization [24]. The only change observed in the shape of the hyperfine magnetic field distribution with respect to that corresponding to the initial amorphous state is a slight shift of the higher peak to lower values.

For Nb and Mo containing samples, the crystalline fractions are estimated at 12 (3) and 16 (4)% respectively, in agreement with those values derived from x-ray patterns. At this stage,

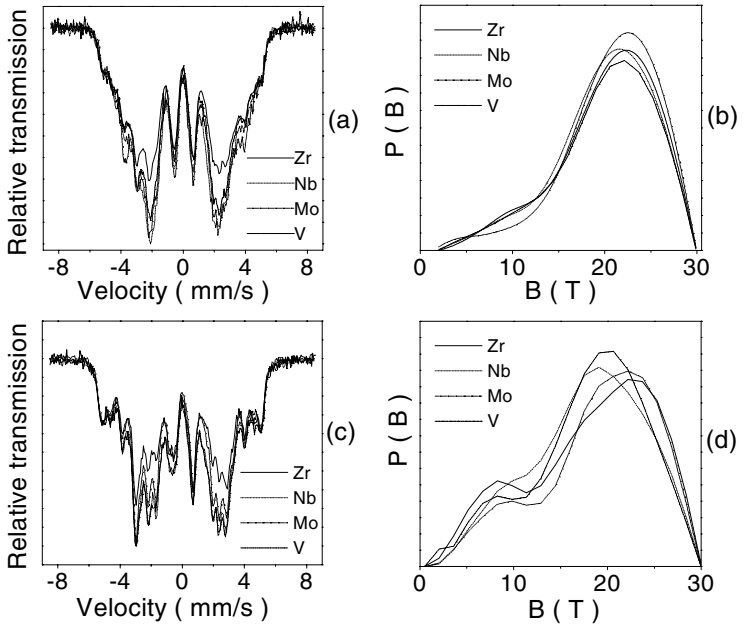

Figure 3. Experimental transmission Mössbauer spectra for nanocrystalline samples of the four compositions with a crystalline fraction of approximately 30 (a) and 50% (c) and their corresponding hyperfine field distributions (b) and (d) respectively.

five crystalline sites are perfectly defined, indicating that the Fe, Si nanocrystallites exhibit already an ordered DO_3 structure. The values of $\langle\theta\rangle$ are approximately the same as those corresponding to the amorphous initial state, slightly superior for the sample containing Nb.

3.3. Intermediate crystalline fraction alloys (>20% and <55%)

An emerging bimodal hyperfine field distribution can be observed for samples of the four compositions for crystalline fractions of approximately ∼20–25%. Figure 3(a) and 3(b) compare the experimental Mössbauer spectra and their corresponding hyperfine field distributions for nanocrystalline samples with crystalline fractions of approximately 30%. At this stage, one observes that the bimodal behaviour is slightly less pronounced for the Mo-based sample. Such a feature is probably due to its less advanced crystallization state, because the atomic diffusion mechanism does not allow two kinds of Fe surroundings to be distinguished at this stage. This point will be discussed below.

A strong change of the hyperfine structure can be observed (figure 3(c)) for samples with crystalline fractions of approximately 55%, when compared with data presented in figure 3(a). In addition, as shown in figure 3(d), the hyperfine field distributions clearly exhibit the occurrence of the bimodal character, as well as a decrease of the high-field hump, i.e. the increase of the low-field peak. Such an evolution can be associated with a lowering of the iron content in the residual amorphous matrix and the increasing number of Fe atoms surrounded by Cu, Nb (X) and B, due to the poor solubility of these elements in the DO_3 Fe, Si phase [27].

Table 3 lists the hyperfine parameters corresponding to the amorphous intergranular phase for samples with crystalline fractions of 30 and 55%. It is clear that the average hyperfine field

Table 3. Hyperfine characteristics of the four nanocrystalline alloys resulting from different thermal treatments leading to crystalline fractions around 30 and 55%, and mean size of corresponding crystalline grains.

X	Treatment	$\langle B \rangle$ (T) ±0.3	Std (T) ±0.3	$\langle \theta \rangle$ (°) ±5	Crystalline fraction (%) ±3	$\langle d \rangle$ (nm) ±2
Zr	773 K—1 h	20.2	5.3	63	28	11
	823 K—5 min	18.1	6.6	68	54	11
Nb	753 K—1 h	19.9	5.2	80	27	12
	798 K—5 min	17.8	5.9	80	54	13
Mo	738 K—1 h	20.7	5.1	63	24	17
	798 K—5 min	18.9	6.1	80	57	17
V	753 K—5 min	20.0	5.4	80	32	20
	773 K—5 min	18.1	5.9	80	54	21

value decreases and the width of the hyperfine field distribution increases when the annealing time and/or the annealing temperature increase, i.e. the crystalline fraction increases.

In other respects, a strong alignment of the magnetic moments parallel to the ribbon plane is clearly evidenced for Nb and V containing samples with a value of $\langle \theta \rangle$ of around 80° that remains constant independently of the crystalline fraction. For the Mo containing sample, the magnetic texture slightly turns from out-of plane to in-plane with increasing crystalline fraction. In contrast, the magnetic texture of the Zr-based alloy is close to being randomly distributed for all crystalline fractions, and is surprisingly similar to that of its initial amorphous state.

3.4. High-crystalline-fraction alloys (>55%)

Figure 4 compares Mössbauer spectra and their corresponding hyperfine field distributions obtained on samples with X = V annealed at 873 K for 5 minutes (a) and X = Nb annealed at 823 K for 60 minutes. For both samples, with a crystalline fraction close to 70%, and by comparing with lower crystalline fraction samples, the following features are found: (i) the bimodal behaviour of the hyperfine field distribution of the intergranular phase is more pronounced, (ii) the mean hyperfine field decreases at the same time that the Curie temperature increases and (iii) a tendency to a random orientation of the magnetic moments. It is important to emphasize that the shape of the hyperfine field distribution is physically realistic although its contribution remains relatively low compared to the crystalline fraction. Indeed we carefully discussed such a point in a previous paper according to the fitting procedure [19].

3.5. Bimodal behaviour of the hyperfine field distributions

The hyperfine field distributions characteristic of the intergranular phase are plotted in figure 5 for as-cast amorphous and nanocrystalline samples with several crystalline fractions for two compositions (X = V and Nb). Similar features are also observed for X = Zr and Mo. Figure 6 shows that the mean values of the hyperfine field decrease with increasing crystalline fraction, being rather independent of the nature of the substituting element X, except for Mo-containing samples, which display slightly larger hyperfine field values. The hyperfine field distributions exhibit a bimodal behaviour which can be roughly described by means of two 'Gaussian' components. Their intensities and positions are dependent on the volumetric

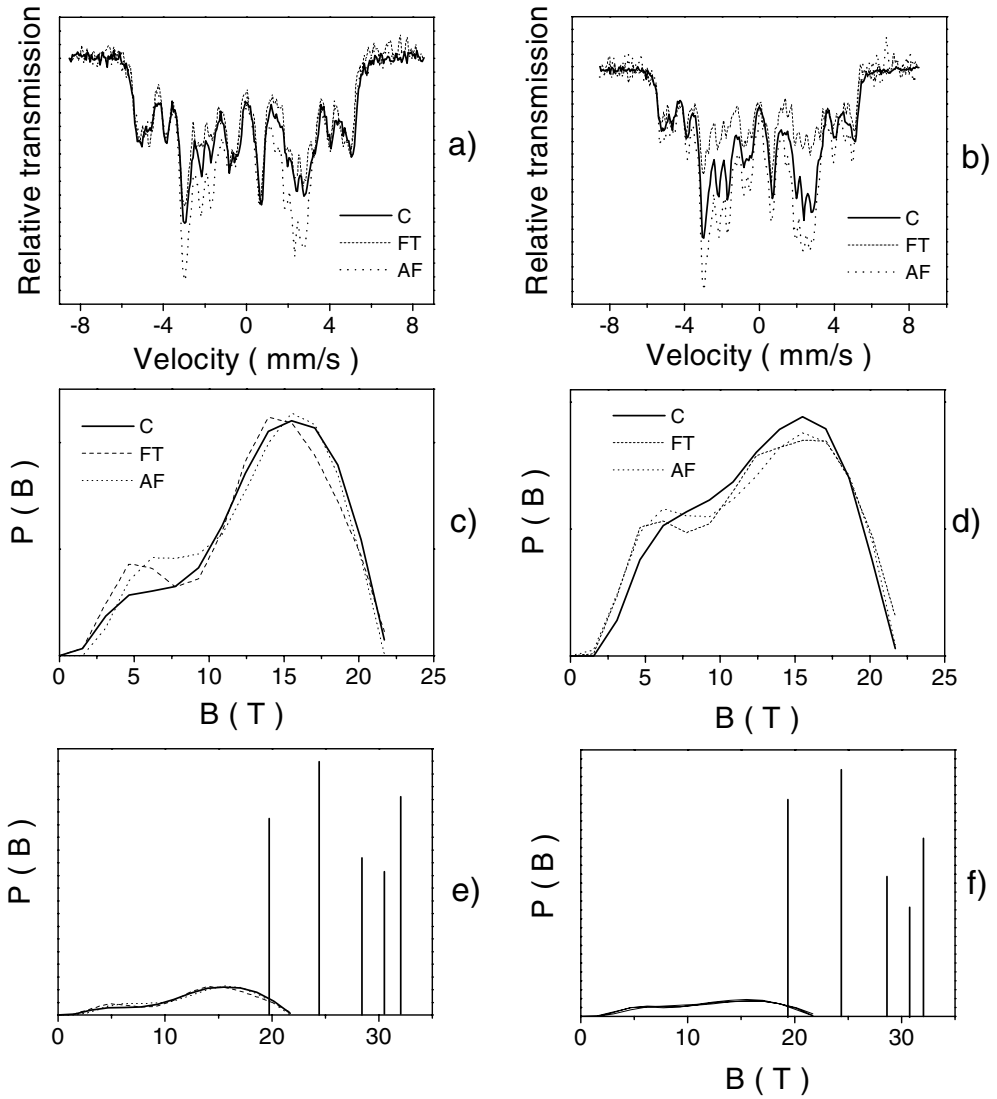

Figure 4. Experimental transmission Mössbauer spectra of samples of the alloys with X = V annealed at 873 K for 5 minutes (a) and with X = Nb annealed at 823 K for 60 minutes (b) obtained in the classic configuration (C), free texture (FT) and with an applied magnetic field (AF) and corresponding hyperfine field distributions (c) and (d), respectively. Figures (e) and (f) compare the intensity of the crystalline components and the amorphous hyperfine field distribution.

crystalline fraction, as shown in figure 7(a). This decomposition is consistent with a two-cluster-like model in agreement with two main kinds of iron environment in the amorphous remainder. It is important to mention that the low peak position was fixed during the refinement for crystalline fractions lower than 20 at.%.

Consequently, two regimes can be distinguished from the shape of the hyperfine field distributions illustrated in figure 5: the bimodal feature remains independent of the crystalline fraction up to values of about 20–25 at.%, whereas for crystalline fractions higher than 20–25 at.% its emergence is clearly observed and it is more pronounced when the crystalline

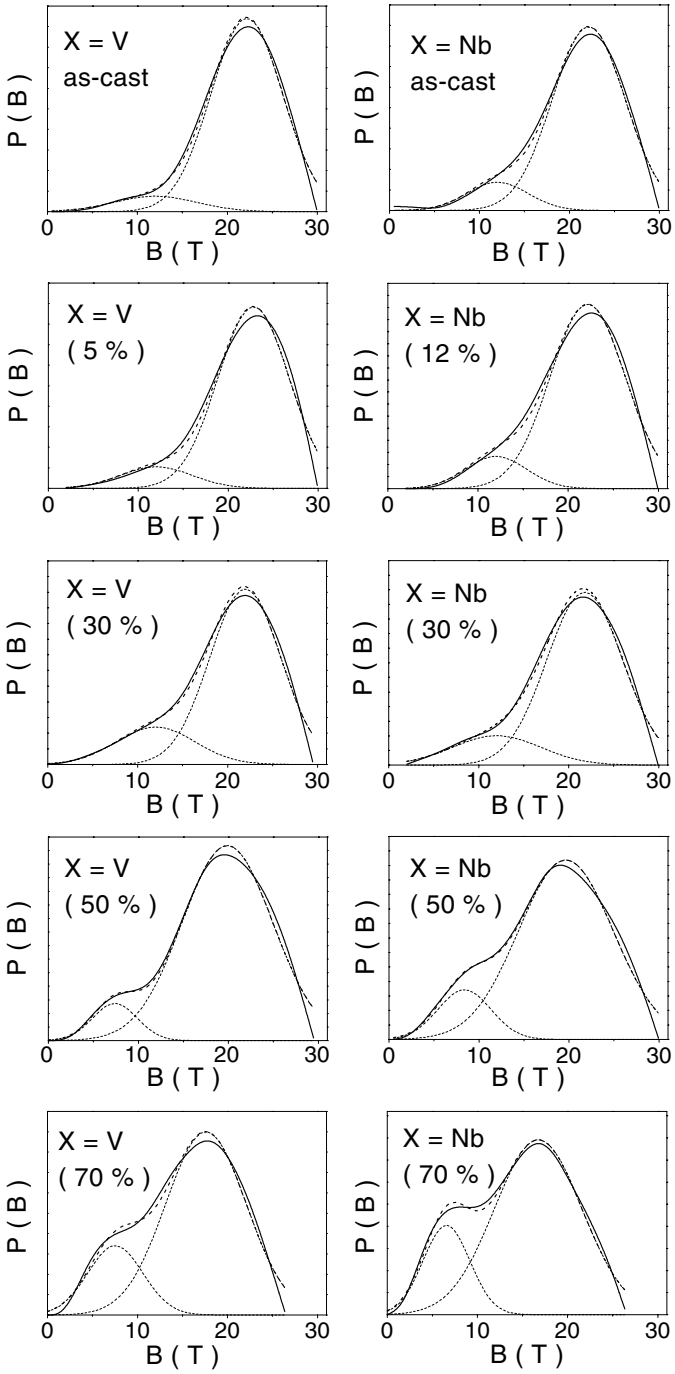

Figure 5. Hyperfine field distributions characteristic of the intergranular phase for as-cast amorphous alloys and nanocrystalline alloys with several crystalline fractions for samples with X = V and Nb.

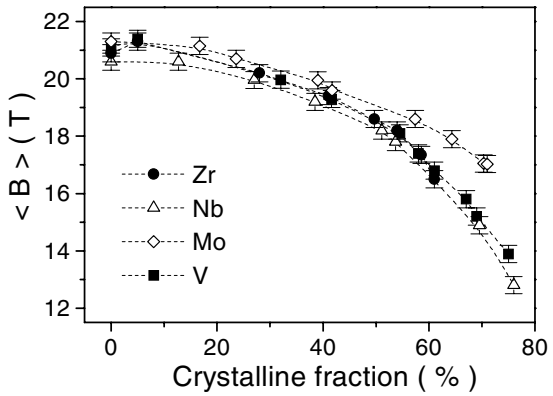

Figure 6. Dependence of the mean hyperfine magnetic field on the crystalline fraction for the four studied alloys.

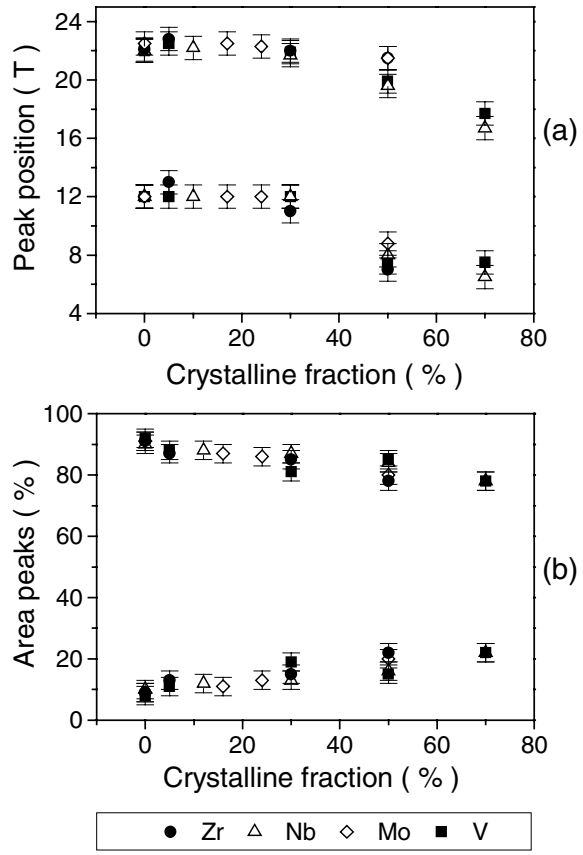

Figure 7. Positions and intensities of the two Gaussian components resulting from the fitting of the hyperfine field distributions of figure 5 versus the crystalline fraction.

fraction increases as shown in figure 5 and 7. The structure of the as-quenched alloy induces an intrinsic bimodal behaviour as previously suggested in [12], although poorly defined, but it is

important to emphasize that the early stage of crystallization, i.e. for low crystalline fraction, it does not significantly affect that behaviour. The more pronounced bimodal character observed for high crystalline fractions can be thus interpreted as due to the emergence of two magnetically distinct types of iron site within the intergranular phase, associated with the nanocrystallization process. High-field values can be attributed to Fe atoms which have preferentially Fe, B and Si atoms as nearest neighbours whereas the low-field component is ascribed to those surrounded by Cu, and X. Indeed, the high-field peak value is close to that encountered in FeB and FeSiB amorphous alloys [28].

The atomic diffusion mechanisms which occur during the annealing treatments favour the emergence of Fe crystalline grains, creating a non-homogeneous chemical amorphous matrix. It is important to emphasize that the compositional changes make the Fe content of the remaining amorphous phase lower than that of the amorphous state. The number of constituents and their different diffusivities make difficult a clear interpretation of the hyperfine field distribution. Nevertheless high contents of refractory element Nb and B atoms have been evidenced by atom probe field ion microscopy (APFIM) at the periphery of crystalline grains in Finemet alloys, that prevent the growth of grains [29]. Consequently the present low-field component might be attributed to iron nuclei located in those regions enriched in X elements. In contrast, the high-field component should be assigned to Fe essentially surrounded by Fe, B and Si located in the 'bulk' of the intergranular region.

The similarity of $P(B)$ curves evidences the similarity in the crystallization process for all these alloys. In addition, it is important to note that the bimodal behaviour of the hyperfine field distribution has been observed in the case of Finemet alloys [12, 15, 30] and less clearly in Nanoperm systems such as FeZrB(Cu), FeNbB(Cu) and FeMoB(Cu) [31], but has not been yet described by means of two Gaussian components, to our knowledge.

4. Conclusions

A special fitting procedure was applied to a series of Mössbauer spectra recorded in different configurations, in order to characterize the component attributed to the crystalline grains and its volumetric crystalline fraction and the hyperfine field distribution of the intergranular phase. A similar behaviour is found for the different alloys for a given crystalline fraction, indicating that the kinetics and the diffusion mechanisms are rather independent of the nature of the substituting X element. A bimodal behaviour of the hyperfine field distributions is clearly evidenced when the crystalline fraction is over $\sim$25 at.%, that is consistent with a non-homogeneous amorphous residual phase. Present results are interpreted in conjunction with those obtained by APFIM: an Fe-poor zone located at the periphery of crystalline grains and an Fe-rich zone preferentially located far from the crystalline grains, consistent with low-field and high-field components, can be distinguished, respectively. Such experimental features have not been observed yet, except in the case of Nanoperm nanocrystalline alloys. The present study allows us to follow, finally, the evolution of the magnetic texture with the crystalline fraction.

Acknowledgments

The authors thank Professor Matyja and the Polytechnical University of Warsaw (Poland) for kindly supplying the ribbons. This work was partially supported by the DGES of the Spanish Ministry of Education (project PB97-1119-CO2-01), by the Picasso French–Spanish Program (HF1998-0211) and by the AECI through the Intercampus Program.

References

[1] Yoshizawa Y, Oguma S and Yamauchi K 1988 *J. Appl. Phys.* **64** 6044
[2] Herzer G 1993 *Phys. Scr.* T **49** 307
[3] Yoshizawa Y and Yamauchi K 1991 *Mater. Sci. Eng.* A **133** 176
[4] Petrovic P, Brovko I, Zemcik T, Zatroch, Konc M, Svec T and Dubovinsky M 1992 *J. Magn. Magn. Mater.* **112** 331
[5] Müller M and Mattern N 1994 *J. Magn. Magn. Mater.* **136** 79
[6] Mattern N, Müller M, Danzing A and Kühn U 1995 *Nanostruct. Mater.* **6** 625
[7] Müller M, Mattern N, Illgen L, Hilzinger H R and Herzer G 1993 *Key Eng. Mater.* **81–83** 221
[8] Borrego J M and Conde A 1997 *Mater. Sci. Eng.* A **226–228** 663
[9] Borrego J M, Peña Rodríguez V A and Conde A, 1997 *Hyperfine Interact.* **110** 1
[10] Hampel G, Pundt A and Hesse J 1992 *J. Phys.: Condens. Matter* **4** 3195
[11] Rixecker G, Schaaf P and Gonser U 1992 *J. Phys.: Condens. Matter* **4** 10 295
[12] Miglierini M 1994 *J. Phys.: Condens. Matter* **6** 1431
[13] Gupta A, Bhagat N and Principi G 1995 *J. Phys.: Condens. Matter* **7** 2237
[14] Pradell T, Clavaguera N, Zhu J and Clavaguera-Mora M T 1995 *J. Phys.: Condens. Matter* **7** 4129
[15] Gorria P, Garitaonandia J S and Barandiaran J M 1996 *J. Phys.: Condens. Matter* **8** 5925
[16] Jiang J Z 1996 *J. Magn. Magn. Mater.* **154** 375
[17] Miglierini M and Greneche J M 1997 *J. Phys.: Condens. Matter* **9** 2303
[18] Greneche J M 1997 *Hyperfine Interact.* **110** 81
[19] Borrego J M, Conde A, Peña Rodríguez V A and Greneche J M *Hyperfine Interact.* submitted
[20] Borrego J M, Conde C F, Millán M, Conde A, Capitán M J and Joulaud J L 1998 *Nanostruct. Mater.* **10** 575
[21] Brand R A, Lauer J and Herlach D M 1983 *J. Phys. F: Met. Phys.* **12** 675
[22] Teillet J and Varret F *MOSFIT Program* University of Le Mans
[23] Greneche J M and Varret F 1982 *J. Phys. C: Solid State Phys.* **15** 5333
[24] Borrego J M, Conde C F and Conde A 2000 *Phil. Mag. Lett.* **80** 359
[25] Zhu J, Clavaguera-Mora M T and Clavaguera N 1997 *Appl. Phys. Lett.* **70** 1709
[26] Garitaonandia J S, Gorria P, Fernández Barquín L and Barandiarán J M 2000 *Phys. Rev.* B **61** 6150
[27] Zemcik T 1993 *Key. Eng. Mater.* **81–83** 261
[28] Stearns M B 1973 *Phys. Rev.* B **8** 4383
[29] Hono K, Hiraga K, Wang Q, Inoue A and Sakurai T 1992 *Acta Metall. Mater.* **40** 2137
[30] Miglierini M, Lipka J and Sitek J 1994 *Hyperfine Interact.* **94** 2193
[31] Miglierini M and Greneche J M 1999 *Hyperfine Interact.* **120–121** 297